LANGMUIR

pubs.acs.org/Langmuir Article

Effect of Ligand Adsorption on the Electronic Properties of the PbS(100) Surface

Abu Asaduzzaman,* Keith Runge, Pierre Deymier, and Krishna Muralidharan

Cite This: https://dx.doi.org/10.1021/acs.langmuir.0c02425 Read Online

ACCESS | Metrics & More | Article Recommendations

ABSTRACT: A first-principles density functional theory calculation was carried out to study the adsorption of acetic acid, methyl amine, methanethiol, and hydrogen iodide on the (100) surface of PbS. All four ligands are common capping agents used in colloidal PbS quantum dot-based photovoltaics. Interestingly, among the considered adsorbates, dissociative adsorption was energetically preferred for hydrogen iodide, while associative adsorption was favorable for the rest. Associative adsorption was driven by strong interactions between the electronegative elements (Y) in the respective ligands and the Pb surface atoms via Pb 6*p*−Y *np* bond hybridization (*n* represents the valence quantum number of the respective electronegative elements). Importantly, the adsorption of ligands altered the work function of PbS, with contrasting trends for associative (decrease in the work function) versus dissociative (increase in the work function) adsorption. The changes in the work function correlates well with a corresponding shift in the 5d level of surface Pb atoms. Other important observations include variations in the work function that linearly change with increasing the surface coverage of adsorbed ligands as well as with the strength of the adsorption of ligands.

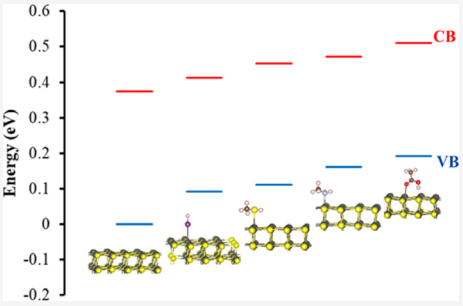

INTRODUCTION

Lead sulfide (PbS) quantum dots (QDs)[1−6] and other colloidal nanocrystals have been a subject of significant research over the last three decades. Quantum confinement in QDs offers synthetic tunability of electronic band gaps and charge mobility and ensuing control over optoelectronic properties via tailoring of the particle size and shape.[7] In addition, the surface chemistry characteristics of PbS QDs are also known to affect both synthesis and their optoelectronic properties.[8−27] In particular, impurities either in precursor, solvent or preparation can significantly affect the performance of PbS QDs, by preferentially binding to the QD surfaces, resulting in trap states that limit the energy conversion efficiencies of these materials. To mitigate trap states and control processing, a variety of organic and inorganic ligands have been deployed, and their effectiveness toward the reduction of surface trap states can be understood and interpreted by characterizing the interactions between ligands and the PbS QDs.

Oleic acid[21] is one of the prominent ligands that is traditionally used to passivate the PbS QDs due to its superior stability and uniform size distribution. However, the long tail oleic acid inhibits the conductivity of PbS QDs.[5] Therefore, short-chain organic molecules containing amine, alcohol, or acid functional groups have been considered as alternatives to oleic acid.[15,22−24] The interactions of ligands (via functional groups) with PbS QDs, in conjunction with ligand−ligand interactions, can be expected to influence many fundamental properties such as, for example, interaction strength, the electronic density of states, and positions of frontier orbitals, which in turn affect the performance of PBS QD-based photovoltaic (PV) devices. For example, it was seen that ligands containing the −OH functional group act as surface traps when adsorbed onto the (111) surface of PbS and lead to detrimental PV performance.[22,25]

In this regard and to provide fundamental insights into the chemical interactions between PbS QDs and ligands, we carry out density functional theory (DFT) calculations, with particular focus on the adsorption mechanisms of the ligands that are used in PbS QDs; the considered ligands include acetic acid, methyl amine, methanethiol, and hydrogen iodide, all of which contain very short tails. Such a choice ensures that our focus remains on characterizing the role of the functional groups. We have used the (100) surface of PbS to examine ligand adsorption since (100) is among the most stable surface orientation of PbS. Using DFT calculations, we endeavor to answer questions on how the different functional groups of ligands influence the properties of PbS QDs. The insights obtained from this work will provide pathways to understand the interplay between the tunability of QD frontier energy

Received: August 16, 2020
Revised: October 9, 2020

levels and adsorption strength and work functions as they relate to ligand identity and coverage.

COMPUTATIONAL METHODS

All calculations have been performed using plane-wave code VASP (version 5.2)[28,29] within the framework of DFT and the generalized gradient approximation (GGA) functional PBE[30] for solids (PBEsol).[31] The projected augmented wave (PAW),[28,32] as provided with the VASP package,[33] is used in this calculation. A cutoff energy of 450 eV was chosen for the plane-wave basis.

While conventional PBE,[30] PBE-D3,[31,34] and PW91[35] functional were used previously for examining PbS,[6,21,26,27,36−38] we have utilized PBEsol[31] due to its ability to accurately reproduce the bulk structural properties of PbS; we note that PBE, PBE-D3, and PW91 overestimate the lattice parameter of PbS. In addition, the calculated work function of the (100) surface using the PBEsol functional is 4.18 eV. The experimental work function[39] values for PbS are 4.34, 4.41, and 4.43 eV at 40, 60, and 80 °C temperatures, respectively. Our calculated work function thus agrees well with the experimental value, given the fact that all calculated properties are at 0 K.

The (100) surface of PbS was obtained from an optimized bulk PbS structure. The simulated (100) slab was represented as a (2 × 2) periodic supercell that was nine atomic layers thick with a vacuum spacing of 20 Å (see Figure 1) separating the periodic images. The

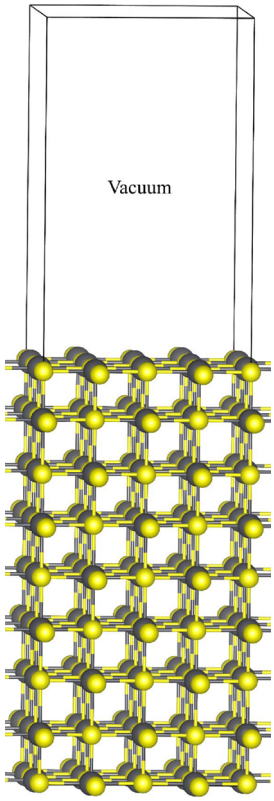

Figure 1. Ball and stick representation of the (100) surface of PbS. The gray and yellow spheres represent Pb and S atoms, respectively. The vertical lines marked the boundary of the supercell.

thickness of the slab corresponded to the critical layer thickness that resulted in invariance in the variation of the energy/PbS unit. To check for this invariance, we systematically examined the energy variation as a function of thickness ranging from 5 to 10 atomic layer thick slabs. We note that most of the earlier studies[6,21,26,27,36,37] used eight or less atomic layer slabs.

For adsorbed surfaces, the effective vacuum region was at least 14.75 Å. Due diligence was performed to avoid any interactions between slabs and greater than separations in previous studies.[21,26,27,36]

For all adsorption studies, the bottom three layers were kept fixed, while all other atoms were allowed to move during the energy minimization routine. The convergence criterion for local energy minima was met when forces on all atoms were smaller than 0.02 eV/Å. A fine grid of 5 × 5 × 1 Monkhorst−Pack[40] k-points was chosen for the calculation.

The adsorption energy of each adsorbate was calculated as follows:

$$\Delta E = \frac{E(n \times \text{adsorbate} \times \text{surface}) - \{E_{\text{surface}} + nE_{\text{adsorbate}}\}}{n} \quad (1)$$

where n is the number of adsorbate molecules and $E(n \times \text{adsorbate} \times \text{surface})$, E_{surface}, and $E_{\text{adsorbate}}$ are the total energies of the energy-minimized adsorbed structure, bare surface, and adsorbate molecule, respectively. The negative and positive values of ΔE signify the stable and unstable sticking of the adsorbate on the surface, respectively.

RESULTS AND DISCUSSION

In this section, we provide data on the adsorption energies of the identified adsorbates, namely, acetic acid, methylamine, methanethiol, and hydrogen iodide. Since it is known that these molecules can dissociate to some extent when in the solvent during the synthesis of PbS QDs, we consider both associative and dissociative adsorption modes.

As a first step toward a thorough characterization of the adsorption process, we provide essential information on both adsorption modes for each molecule in Table 1, while the

Table 1. Mode of the Adsorption of Ligands on the (100) Surface of PbS

adsorbate	adsorption modes	description	stability (based on adsorption energetics)
amine: CH_3NH_2	associative	NH_2 group attaches to a surface Pb atom	stable
	dissociative	NH group attaches to a surface Pb atom and H attaches to surface S atoms	unfavorable
thiol: CH_3SH	associative	SH group attaches to a surface Pb atom	stable
	dissociative	S attaches to a surface Pb atom and H attaches to a surface S atom	unfavorable
acid: CH_3COOH	associative	−O and −OH attach to surface Pb and S atoms, respectively	stable
	dissociative	COO attaches to two surface Pb atoms and H to surface S atoms	unfavorable
iodide: HI	associative	HI (via I) attaches to a surface Pb atom	stable
	dissociative	H and I attach to surface S and Pb atoms, respectively	stable

energetics of adsorption is provided in Table 2. Further, the respective adsorption geometries are provided in Figure 2, while Figure 3 provides the dissociative adsorption geometry of HI. In particular, we note that amongst all adsorbates, both adsorption modes are energetically favorable only for HI. For other adsorbates, associative adsorption is favored, while dissociative adsorption is energetically unfavorable. Further, in Table 2, we also provide the variations in the adsorption energies as a function of surface coverage for each species. Table 2 indicates that, with the exception of HI, the adsorption energy/molecule increases (i.e., becomes less negative) with increasing coverage.

https://dx.doi.org/10.1021/acs.langmuir.0c02425
Langmuir XXXX, XXX, XXX−XXX

Table 2. Adsorption Energy, ΔE in kJ/mol for Each Molecule of Adsorbate at Different Coverages

	adsorbate				
	associative				dissociative
coverage	CH_3COOH	CH_3NH_2	CH_3SH		HI
1/8	−58.30	−54.98	−31.77	−9.46	−73.74
1/4	−55.62	−49.39	−30.33	−12.13	−65.64
1/2	−51.64	−42.43	−29.12	−14.46	−45.98
1	−51.53	−36.53	−25.81	−18.60	−45.92

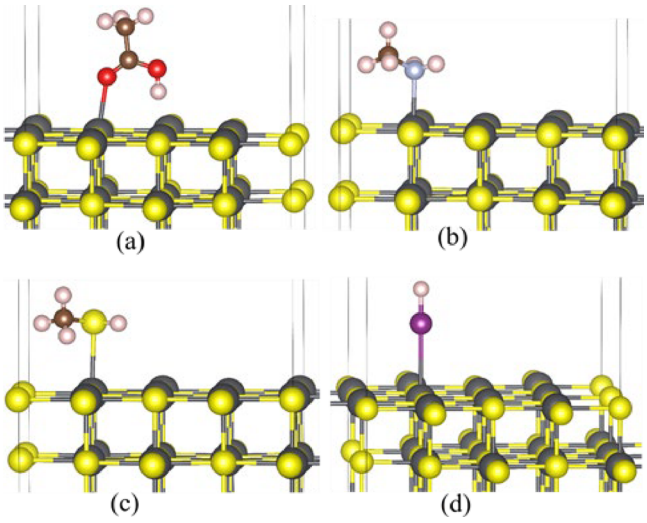

Figure 2. Molecular adsorption of (a) acetic acid, (b) methyl amine, (c) methanethiol, and (d) hydrogen iodide. A coverage of 1/8 is represented in each case. The brown, red, silver, white, and purple spheres represent C, O, N, H, and I atoms, respectively. The other representation is the same as that of Figure 1.

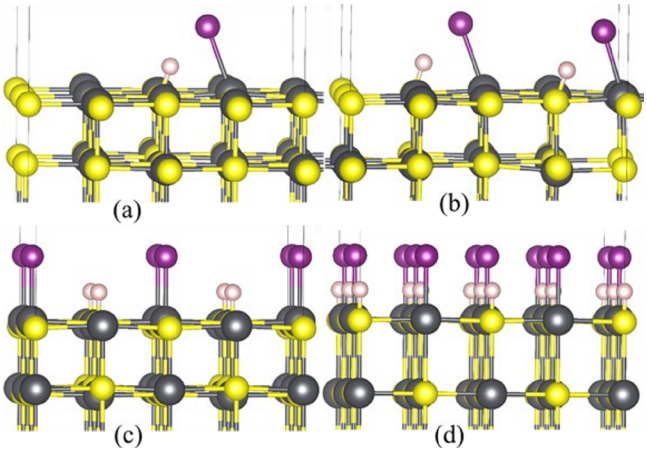

Figure 3. Dissociative adsorption of HI on the (100) surface of PbS for coverage of (a) 1/8, (b) 1/4, (c) 1/2, and (d) 1 (full). The representation is the same as that of Figure 2.

To provide a fundamental understanding of the listed observations, namely, (i) associative adsorption is energetically favorable for all adsorbates, whereas dissociative adsorption is energetically favorable only for HI, and (ii) adsorption strength/molecule becomes weaker with increasing surface coverage; with the notable exception of HI, we first focus on the associative adsorption of the ligands.

As evident from Figure 2 and as noted in Table 1, it is clear that to saturate the dangling bonds; surface Pb atoms prefer "association" with the respective electronegative atoms corresponding to each adsorbate, namely, O (for acetic acid), S (for methanethiol), N (for methylamine), and I for (hydrogen iodide). Further, in the case of acetic acid, there are additional interactions between a surface S atom and the OH moiety in acetic acid. The electronegativities of O and N are much higher than those of S and I, and this is reflected in the fact that the adsorption strength of acetic acid is the highest followed by methyl amine. Although the electronegativities of S and I are very similar, the electron-donating group on CH_3SH makes the S atom more electron rich and leads to strong adsorbate (S)−adsorbent (Pb) interactions as compared to HI. Thus, from a molecular adsorption point of view, HI demonstrates the weakest associative adsorption strength amongst all the considered adsorbates. However, with increasing surface coverage, the fact that the adsorption strength (i.e., adsorption energy/molecule) decreases for all adsorbates other than HI can be correlated with steric effects that come into play; for HI, the increase in the adsorption strength with increasing surface coverage is attributed to the lack of significant steric effects due to the "vertical" adsorption geometry of HI coupled with synergistic hydrogen bonding effects as more HI molecules adsorb on the surface. We also note that the reported adsorption energies for CH_3NH_2 at 1/4 and 1/2 surface coverage are slightly higher than the respective values reported previously.[37] These discrepancies of the adsorption energy might stem from the fact that slightly overestimated lattice parameters were used previously, which would reduce the above-mentioned steric repulsion.

To illustrate the above observations especially for the single molecule-adsorption, we present the respective electron density plots for the adsorption geometries of the different adsorbates in Figure 4. Consistent with our observations, there is clear evidence of charge transfer between the surface Pb atoms and the corresponding electronegative atoms of the

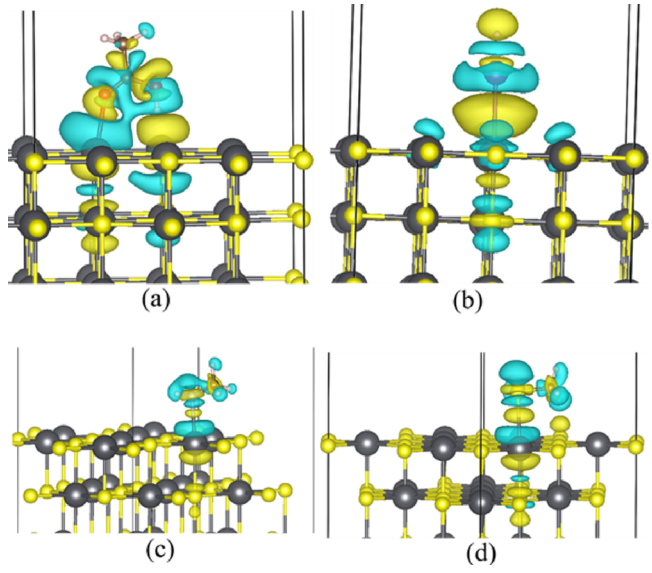

Figure 4. Illustration of loss (blue) and gain (yellow) of electron density during the associative adsorption of (a) acetic acid, (b) HI, (c) methylamine, and (d) methanethiol. The representation is the same as that of Figure 2.

https://dx.doi.org/10.1021/acs.langmuir.0c02425
Langmuir XXXX, XXX, XXX−XXX

ligands. The respective Bader charges[41−43] on the Pb and the electronegative atoms are provided in Table 3, which is consistent with the adsorption strength trends. Also, we note that while a single locus of electron density exchange is observed for CH_3NH_2, CH_3SH, and HI with the PbS surface, there are two such exchanges for CH_3COOH, corresponding to (i) O and surface Pb and (ii) OH and surface S.

Table 3. Bader Charge[41−43] on Interacting Surface Pb and Electronegative Atoms of Ligands for the Adsorption of 1/8 Surface Coverage

	Bader charges	
ligands	Pb	O/N/S/I
CH_3COOH	1.07^+	1.19^-
CH_3NH_2	0.93^+	1.15^-
CH_3SH	0.86^+	0.05^-
HI	0.95^+	0.01^-

To provide further insights into the bonding between the adsorbates and the surface, we analyze the respective electronic density of states (DOS), as given in Figure 5. In particular, Figure 5 shows a distinct hybridization between the 6p orbitals of Pb and the valence p orbitals of the electronegative atoms of the adsorbate. Further, the hybridization between the Pb 6p orbitals and 2p orbitals of O (5a)/N (5b), and 3p orbitals of S (5c) and 5p orbitals of I (5d) atoms manifests as a corresponding DOS feature between −5 to 0 eV (Figure 5).

In the case of dissociative adsorption, we note that for acetic acid, methylamine, and methanethiol, dissociative adsorption was not viable chiefly due to the presence of the methyl group, which led to energetically unfavorable interactions. However, in the case of HI, aided by the relatively weaker H−I bond and favorable bonding between surface Pb and I as well as surface S with H, dissociative adsorption was energetically much more stable as compared to associative adsorption. However, with increasing surface coverage, for the dissociative adsorption case, we see that adsorption strength/molecule becomes weaker, which is directly attributed to the respective adsorption geometries. In particular, for the case of a single HI molecule, the adsorbed H and I atoms form bonds with the S and Pb atoms of the surface, with the bond oriented at an angle to the surface normal. With increasing coverage, due to geometric effects, the orientation of the bonds becomes parallel to the surface normal, deviating from the preferred orientation for the single molecule, leading to a consequent decrease in the adsorption strength. Nevertheless, it is worth pointing out that dissociative adsorption is always energetically preferred for HI for all surface coverages.

Having provided a detailed analysis of the adsorption energetics and preferred geometries, we turn our attention to understanding the interplay among adsorption, band structure, and work function of the adsorbed systems. Importantly, the band gap of PbS does not change significantly due to the adsorption of ligands (± 0.06 eV). However, the positions of frontier orbitals or equivalently the positions of the valence band and the conduction band move upward (with respect to a fixed vacuum level), as shown in Figure 6 and in agreement with a previous report.[26] The band edges of the frontier orbitals shift progressively from the pristine surface to the different associatively adsorbed systems, namely (and in order): HI-adsorbed, methanethiol-adsorbed, methyl amine-adsorbed, and acetic acid-adsorbed surfaces, consistent with the trends observed in the adsorption energies. For the

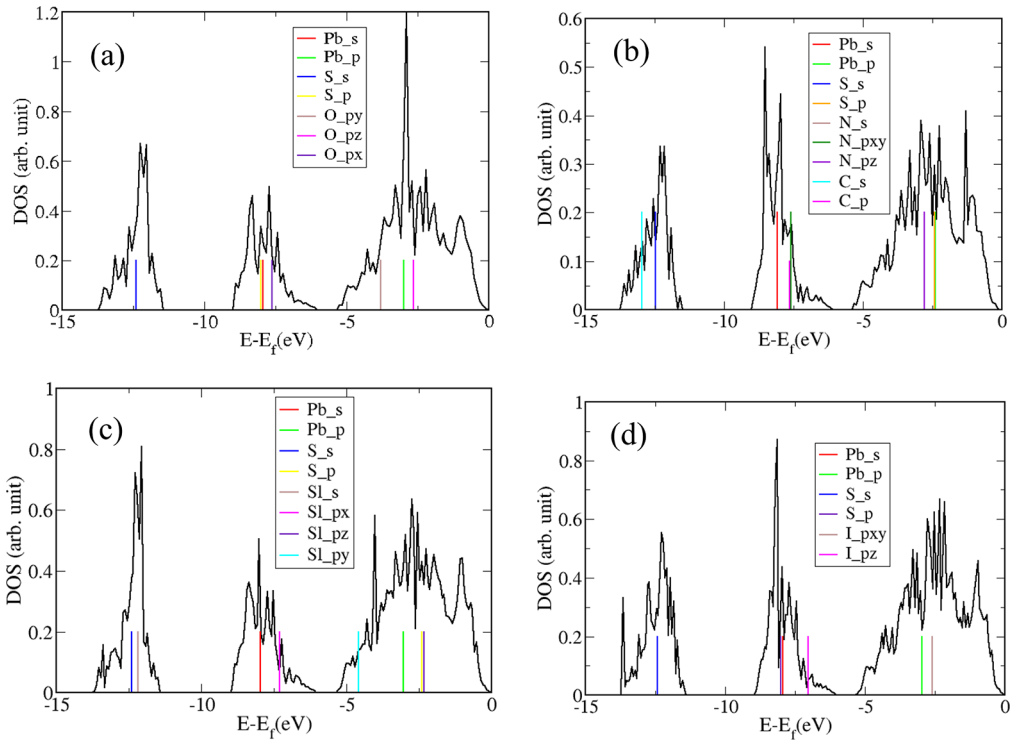

Figure 5. Density of states (DOS) for the adsorption of (a) acetic acid, (b) methyl amine, (c) methanethiol, and (d) HI. The average of each respective band (s, p, p_x, p_y, and p_z) is represented by a vertical line. The sulfur atoms in the surface and ligand are differentiated by S and Sl, respectively, in (c).

https://dx.doi.org/10.1021/acs.langmuir.0c02425
Langmuir XXXX, XXX, XXX−XXX

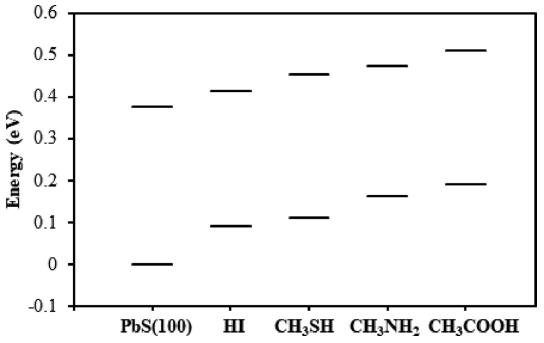

Figure 6. Position of the band edges of the valence band (lower panel) and the conduction band (upper panel) for the PbS(100) surface and PbS(100) with adsorbates such as hydrogen iodide (HI), methane thiol (CH_3SH), methyl amine (CH_3NH_2), and acetic acid (CH_3COOH). For the PbS(100) surface, the band positions are determined by $E_s - E_f$ (E_s and E_f are the band and Fermi energy, respectively, in PbS(100)). To highlight the band shift in adsorbed systems with respect to that of surface, the band positions are normalized by $E_a - E_f$ (E_a is the band energy in the adsorbate) in the adsorbed systems.

dissociated HI case, the shift is downward in direct contrast to the associated adsorption systems.

The work function is defined as the minimum energy required to remove an electron from the surface to the vacuum. Traditionally, the work function is calculated as the energy difference between the Fermi level and the vacuum level.[44] Here, the work function for bulk PbS(100) has been calculated as 4.18 eV. Yeon et al.[39] experimentally determined the work function of PbS processed at different temperatures with values of 4.34, 4.41, and 4.43 eV for PbS processed at 40, 60, and 80 °C temperatures, respectively. Thus, the 0 K calculated value of 4.18 eV can be inferred to be in good agreement with the experiment. The calculated work function for PbS(100) with surface adsorbates is summarized in Table 4.

Table 4. Work Function in eV for the Adsorbate-Covered PbS(100) Surface[a]

	adsorption				
	associative				dissociative
coverage	CH_3COOH	CH_3NH_2	CH_3SH		HI
1/8	3.82	3.95	3.97	4.02	4.53
1/4	3.72	3.80	3.83	4.01	4.79
1/2	3.43	3.60	3.65	3.92	5.14
1	3.27	3.37	3.46	3.68	5.16

[a]The work function of the pristine PbS(100) surface is 4.18, which is close to the experimental values of 4.34 at 40 °C.[39]

There are a few characteristic features that emerge from the work function calculations: (a) work function for associatively adsorbed surface is lower than that of the pure surface, (b) the work function decreases with increasing surface coverage, (3) the work function of the dissociated adsorption surface (using HI as reference) is higher than that of the pure surface, and (4) the work function decreases as the adsorption energy decreases.

The lowering of the work function ($\Delta\Phi$) upon adsorption can be explained in terms of the change in the dipole moment of the PbS(100) surface ($\Delta\mu$) upon adsorption of molecules as[45]

$$\Delta\Phi = \frac{e\Delta\mu}{\epsilon_0 A} \quad (2)$$

where A is the adsorbate surface area and $\Delta\mu$ is the change in the dipole moment upon adsorption normal to the surface. In particular, for associative adsorption, the electronegative atoms of the adsorbate point inwards (toward the surface) while the surface dipole points away from the surface, leading to countering the dipole moment of the surface (see Figure 7).

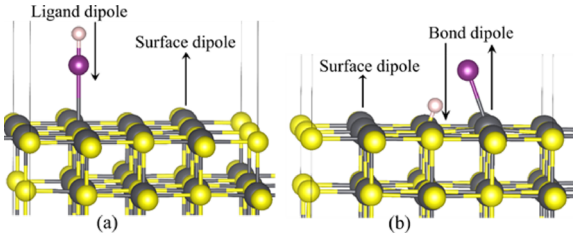

Figure 7. Dipole direction of the ligand, bond, and surface. HI is a representative example: (a) associative adsorption and (b) dissociative adsorption of HI. The representation is the same as that of Figure 2.

The $\Delta\mu$ values of the adsorption is thus negative, resulting in the lowering of the work function of the adsorbed surface with respect to the pristine surface, with this effect further accentuated with increasing surface coverage.

On the other hand, during the dissociative adsorption of HI, the stronger bond dipole for Pb−I is aligned with the surface dipole, whereas the weaker S−H dipole is antialigned. As a result, there is a net increase in the total dipole of this system (i.e., HI dissociative adsorption on the PbS(100) surface). Our calculated results on the work function and their relation to the dipole moments are consistent with the previously reported observations.[44]

To further discuss the electronic structure, the surface core-level shift of the Pb 5d orbital has been calculated. The energy that is required to remove a core electron from an atom is called a core-level binding energy. The electrons are excited by X-ray photons experimentally, and usually the binding energies are specified relative to the Fermi energy. Due the different local environment at the surface, the core-level binding energy of surface atoms shifts from bulk. This shift of the core-level binding energy for the surface atoms is called surface core-level shift (E_{SCLS}).[46] Using the initial state approximation, the E_{SCLS} for the surface Pb 5d level has been calculated and is shown in Table 5.

The calculated E_{SCLS} values for all adsorbates follow: (a) the E_{SCLS} increases with increasing coverage for molecular adsorption and (b) the E_{SCLS} decreases with increasing coverage for dissociated adsorption. The calculated trends for

Table 5. Shift of the 5d Level of Surface Pb in eV for the Adsorbate-Covered PbS(100) Surface

	adsorbate				
	associative				dissociative
coverage	CH_3COOH	CH_3NH_2	CH_3SH		HI
1/8	0.42	0.34	0.26	0.14	−0.22
1/4	0.51	0.46	0.43	0.17	−0.47
1/2	0.78	0.65	0.57	0.22	−0.66
1	0.94	0.83	0.67	0.33	−0.75

https://dx.doi.org/10.1021/acs.langmuir.0c02425
Langmuir XXXX, XXX, XXX−XXX

E_{SCLS} nicely complement the work function data presented above. As the core electrons bind tightly (higher E_{SCLS}), the valence electrons are easier to remove (smaller work functions).

The correlation of the work function and the E_{SCLS} can be further investigated by calculating the depression of the work function due to adsorption. The depression of work function (Φ_d) due to adsorption is calculated as follows:

$$\Phi_d = \Phi_{surf} - \Phi_{ads} \quad (3)$$

where Φ_{surf} and Φ_{ads} are the work functions for the pristine surface and adsorbed systems, respectively. Figure 8 shows the variation of Φ_d and E_{SCLS} with surface coverage. For each ligand, the E_{SCLS} and Φ_d are correlated with each other. The slight deviation of E_{SCLS} from Φ_d is due to the local charge distribution. The dissociated adsorption of HI, although works opposite to associative adsorption, follows the same correlation between E_{SCLS} and Φ_d.

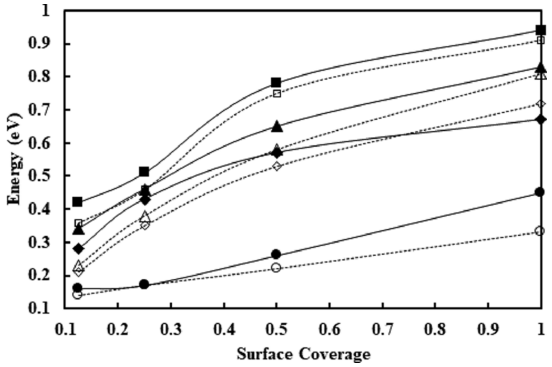

Figure 8. Binding energy shift of the surface layer Pb 5d orbitals (solid lines/closed symbols) and the depression of the work function (dashed lines/open symbol) of the adsorbed surface from its pristine surface ($\Phi_d = \Phi_{surf} - \Phi_{ads}$). Symbol: square = acetic acid, triangle = methyl amine, diamond = methanethiol, and circle = HI.

CONCLUSIONS

Four short tail common ligands, acetic acid, methyl amine, methanethiol, and hydrogen iodide, are used to study how strongly they bind to the (100) surface of PbS, the most stable surface for PbS QDs. Although the associative adsorption of all four ligands are thermodynamically favorable, the dissociative adsorption of only HI is thermodynamically favorable. The adsorption energy of the dissociative adsorption of HI is much stronger than that of associative adsorption. The mode of adsorption (associative or dissociative) of ligands depends on the bond polarity of the linking atoms of the ligand. In the adsorption process, the 6p orbitals of the surface Pb atom hybridize with the valence p orbitals of the electronegative atoms of the ligand. The adsorption of ligands on the PbS(100) surface modifies the electronic properties of the adsorbent. While the band gap is essentially similar for both the pristine and adsorbed surface, the band edges of the frontier orbitals progressively shift upward with adsorption strength. The work function decreases for the associative adsorption, whereas the work function increases for dissociative adsorption. The work function of adsorbed surfaces changes linearly with surface coverage. The deviation of the dipole moment of the adsorbed surface from the pristine-unadsorbed system determines the change in the work function. The surface core-level shift of Pb 5d levels correlates well with the observed shifts in work functions and serves as a complementary measure to confirm the work function vs adsorption trends. The electronegativity of the linking atoms of ligands ultimately controls the properties of PbS: the higher the electronegativity, the stronger the interaction with the surface; the stronger the interaction, the lower the work function; the higher the surface coverage, the lower the work function; and the stronger the interaction, the higher the shift of frontier orbitals.

Although PV devices based on PbS QDs are very promising, solution-processed PV devices have a few limitations including surface trap states, which limit the energy conversion efficiency and the stability of devices in air. The capping of QDs by ligands limits the surface trap states and thereby improves the energy conversion efficiency. Similarly, the ligands work against the oxidation and thereby improve the air stability of devices. Further, the stability also directly correlates with the number of capping agents. Band edge shifts due to ligand capping can be used to harvest energy in the wider range of the solar spectrum for single and multijunction solar cells. This study thus provides valuable guidance to the experimentalist to choose the right type and number of ligands for designing PbS-based PV that can harvest at multiple wavelengths with improved device stability as design criteria.

AUTHOR INFORMATION

Corresponding Author

Abu Asaduzzaman − *School of Science, Engineering and Technology, Pennsylvania State University − Harrisburg, Middletown, Pennsylvania 17057, United States;* orcid.org/0000-0002-6385-3014; Email: aua1309@psu.edu

Authors

Keith Runge − *Materials Science and Engineering, University of Arizona, Tucson, Arizona 85721, United States*

Pierre Deymier − *Materials Science and Engineering, University of Arizona, Tucson, Arizona 85721, United States*

Krishna Muralidharan − *Materials Science and Engineering, University of Arizona, Tucson, Arizona 85721, United States*

Complete contact information is available at: https://pubs.acs.org/10.1021/acs.langmuir.0c02425

Notes

The authors declare no competing financial interest.

ACKNOWLEDGMENTS

All calculations were performed at the High Performance Computing, University of Arizona (UA HPC). A.A. acknowledges the "startup" support from Penn State Harrisburg.

REFERENCES

(1) Alivisatos, A. P. Semiconductor Clusters, Nanocrystals, and Quantum Dots. *Science* **1996**, *271*, 933−937.

(2) Kovalenko, M. V.; Manna, L.; Cabot, A.; Hens, Z.; Talapin, D. V.; Kagan, C. R.; Klimov, V. I.; Rogach, A. L.; Reiss, P.; Milliron, D. J.; Guyot-Sionnnest, P.; Konstantatos, G.; Parak, W. J.; Hyeon, T.; Korgel, B. A.; Murray, C. B.; Heiss, W. Prospects of Nanoscience with Nanocrystals. *ACS Nano* **2015**, *9*, 1012−1057.

(3) Bronstein, N. D.; Martinez, M. S.; Kroupa, D. M.; Vörös, M.; Lu, H.; Brawand, N. P.; Nozik, A. J.; Sellinger, A.; Galli, G.; Beard, M. C. Designing Janus Ligand Shells on PbS Quantum Dots using Ligand−Ligand Cooperativity. *ACS Nano* **2019**, *13*, 3839−3846.

https://dx.doi.org/10.1021/acs.langmuir.0c02425
Langmuir XXXX, XXX, XXX−XXX

(4) Ngo, T. T.; Masi, S.; Mendez, P. F.; Kazes, M.; Oron, D.; Seró, I. M. PbS quantum dots as additives in methylammonium halide perovskite solar cells: the effect of quantum dot capping. *Nanoscale Adv.* **2019**, *1*, 4109−4118.
(5) Dastjerdi, H. T.; Prochowicz, D.; Yadav, P.; Tavakoli, M. M. Synergistic ligand exchange and UV curing of PbS quantum dots for effective surface passivation. *Nanoscale* **2019**, *11*, 22832−22840.
(6) Kroupa, D. M.; Voros, M.; Brawand, N. P.; McNichols, B. W.; Miller, E. M.; Gu, J.; Nozik, A. J.; Sellinger, A.; Galli, G.; Beard, M. C. Tuning colloidal quantum dot band edge positions through solution-phase surface chemistry modification. *Nat. Commun.* **2017**, *8*, 15257.
(7) Teh, Z. L.; Hu, L.; Zhang, Z.; Gentle, A. R.; Chen, Z.; Gao, Y.; Yuan, L.; Hu, Y.; Wu, T.; Patterson, R. J.; Huang, S. Enhanced Power Conversion Efficiency via Hibrid Ligand Exchange Treatment of p-Type PbS Quantum Dots. *ACS Appl. Mater. Interfaces* **2020**, *12*, 22751−22759.
(8) Harris, R. D.; Homan, S. B.; Kodaimati, M.; He, C.; Nepomnyashchii, A. B.; Swenson, N. K.; Lian, S. C.; Calzada, R.; Weiss, E. A. Electronic Processes within Quantum Dot-Molecule Complexes. *Chem. Rev.* **2016**, *116*, 12865−12919.
(9) Mandal, D.; Goswami, P. N.; Rath, A. K. Thiol and Halometallate, Mutually Passivated Quantum Dot Ink for Photovoltaic Application. *ACS Appl. Mater. Interfaces* **2019**, *11*, 26100−26108.
(10) Clark, R. C. J.; Neo, D. C.; Ahumada-Lazo, R.; Williamson, A.; Pis, I.; Nappini, S.; Watt, A. A. R.; Flavell, W. R. Influence of Multistep Surface Passivation on the Performance of PbS Colloidal Quantum Dot Solar Cells. *Langmuir* **2018**, *34*, 8887−8897.
(11) Cai, J.; Miao, Y. Q.; Yu, B. Z.; Ma, P.; Fan, H. M. Large-Scale, Facile Transfer of Oleic Acid-Stabilized Iron Oxide Nanoparticles to the Aqueous Phase for Biological Applications. *Langmuir* **2017**, *33*, 1662−1669.
(12) Kang, J.; Park, D.; Kim, J.; Eom, S. H.; Jang, S.-Y.; Yim, S.; Jung, I. H. Improved performance of Quantum-Dot Photodetectors Using Cheap and Environmentally Friendly Polyethylene Glycol. *Adv. Mater. Interfaces* **2019**, *6*, 1801666.
(13) Ueda, S. T.; Kwak, I.; Abelson, A.; Wolf, S.; Qian, M.; law, M.; Kummel, A. C. Electronic passivation of PbSe quantum dot solids by trimethylaluminum vapor dosing. *Appl. Surf. Sci.* **2020**, *513*, 145812.
(14) Hendricks, M. P.; Campos, M. P.; Cleveland, G. T.; Plante, I. J.-L.; Owen, J. S. A Tunable Library of Substituted Thiourea Precursors to Metal Sulfide Nanocrystals. *Science* **2015**, *348*, 1226−−1230.
(15) Crisp, R. W.; Kroupa, D. M.; Marshall, A. R.; Miller, E. M.; Zhang, J.; Beard, M. C.; Luther, J. M. Metal Halide Solid-State Surface Treatment for High Efficiency PbS and PbSe Qd Solar Cells. *Sci. Rep.* **2015**, *5*, 9945.
(16) Widmer-Cooper, A.; Geissler, P. L. Ligand-Mediated Interactions between Nanoscale Surfaces Depend Sensitively and Nonlinearly on Temperature, Facet Dimensions, and Ligand Coverage. *ACS Nano* **2016**, *10*, 1877−1887.
(17) Giansante, C.; Infante, I.; Fabiano, E.; Grisorio, R.; Suranna, G. P.; Gigli, G. Darker-Than-Black PbS Quantum Dots: Enhancing Optical Absorption of Colloidal Semiconductor Nanocrystals Via Short Conjugated Ligands. *J. Am. Chem. Soc.* **2015**, *137*, 1875−1886.
(18) Kroupa, D. M.; Voros, M.; Brawand, N. P.; Bronstein, N.; Mcnichols, B. W.; Castaneda, C.; Nozik, A. J.; Sellinger, A.; Galli, G.; Beard, M. C. Optical Absorbance Enhancement in Pbs QD/Cinnamate Ligand Complexes. *J. Phys. Chem. Lett.* **2018**, *9*, 3425−3433.
(19) Goswami, B.; Pal, S.; Sarkar, P. Theoretical studies of the effect of surface passivation on structural, electronic, and optical properties of zinc selenide clusters. *Phys. Rev. B* **2007**, *76*, No. 045323.
(20) Saha, S.; Sarkar, S.; Pal, S.; Sarkar, P. Ligand mediated tuning of the electronic energy levels of ZnO nanoparticles. *RSC Adv.* **2013**, *3*, 532.
(21) Zherebetskyy, D.; Scheele, M.; Zhang, Y.; Bronstein, N.; Thompson, C.; Britt, D.; Salmeron, M.; Alivisatos, P.; Wang, L.-W. Hydroxylation of the surface of PbS nanocrystals passivated with oleic acid. *Science* **2014**, *344*, 1380−1384.
(22) Chuang, C.-H. M.; Brown, P. R.; Bulović, V.; Bawendi, M. G. Improved performance and stability in quantum dot solar cells through band alignment engineering. *Nat. Mater.* **2014**, *13*, 796−801.
(23) Tang, J.; Kemp, K. W.; Hoogland, S.; Jeong, K. S.; Liu, H.; Levina, L.; Furukawa, M.; Wang, X.; Debnath, R.; Cha, D.; Chou, K. W.; Fischer, A.; Amassian, A.; Asbury, J. B.; Sargent, E. H. Colloidal-quantum-dot photovoltaics using atomic-ligand passivation. *Nat. Mater.* **2011**, *10*, 765−771.
(24) Zhitomirsky, D.; Voznyy, O.; Hoogland, S.; Sargent, E. H. Measuring Charge Carrier Diffusion in Coupled Colloidal Quantum Dot Solids. *ACS Nano* **2013**, *7*, 5282−5290.
(25) Yang, X.; Yang, J.; Khan, J.; Deng, H.; Yuan, S.; Zhang, J.; Xia, Y.; Deng, F.; Zhou, X.; Umar, F.; Jin, X.; Song, H.; Cheng, C.; Sabry, M.; Tang, J. Hydroiodic Acid Additive Enhanced the Performance and Stability of PbS-QDs Solar Cells via Suppressing Hydroxyl Ligand. *Nano-Micro Lett.* **2020**, *12*, 37.
(26) Brown, P. R.; Kim, D.; Lunt, R. R.; Zhao, N.; Bawendi, M. G.; Grossman, J. C.; Bulovic, V. Energy Level Modification in Lead Sulfide Quantum Dot Thin Films through Ligand Exchange. *ACS Nano* **2014**, *8*, 5863−5872.
(27) Kim, D.; Kim, D.-H.; Lee, J.-H.; Grossman, J. C. Impact of Stoichiometry on the Electronic Structure of PbS Quantum Dots. *Phys. Rev. Lett.* **2013**, *110*, 196802.
(28) Kresse, G.; Furthmüller, J. Efficiency of Ab-Initio Total Energy Calculation for Metals and Semiconductors Using Plane-Wave Basis Set. *Comput. Mater. Sci.* **1996**, *6*, 15−50.
(29) Kresse, G.; Joubert, D. From Ultrasoft Pseudopotentials to the Projector Augmented-Wave Method. *Phys. Rev. B* **1999**, *59*, 1758−1775.
(30) Perdew, J. P.; Burke, K.; Ernzerhof, M. Generalized Gradient Approximation Made Simple. *Phys. Rev. Lett.* **1996**, *77*, 3865−3868.
(31) Perdew, J. P.; Ruzsinszky, A.; Csonka, G. I.; Vydrov, O. A.; Scuseria, G. E.; Constantin, G. E.; Zhou, X.; Burke, K. Restoring the Density-Gradient Expansion for Exchange in Solids and Surfaces. *Phys. Rev. Lett.* **2008**, *100*, 136406.
(32) Blöchl, P. E. Projector Augmented-Wave Method. *Phys. Rev. B* **1994**, *50*, 17953−17979.
(33) Kresse, G.; Hafner, J. Norm-Conserving and Ultrasoft Pseudopotentials for First-Row and Transition Elements. *J. Phys.: Condens. Matter* **1994**, *6*, 8245.
(34) Grimme, S.; Antony, J.; Ehrlich, S.; Krieg, H. A consistent and accurate ab initio parametrization of density functional dispersion correction (DFT-D) for the 94 elements H-Pu. *J. Chem. Phys.* **2010**, *132*, 154104.
(35) Perdew, J. P.; Wang, Y. Accurate and simple analytic representation of the electron-gas correlation energy. *Phys. Rev. B* **1992**, *45*, 13244.
(36) Chen, J.; Long, X.; Chen, Y. Comparison of Multilayer Water Adsorption on the Hydrophobic Galena (PbS) and Hydrophilic Pyrite (FeS2) Surfaces: A DFT Study. *J. Phys. Chem. C* **2014**, *118*, 11657−11665.
(37) Zhang, L.; Song, Q.; Zhang, S. B. Exceptionally Strong Hydrogen Bonds Affect the Surface Energy of Colloidal Nanocrystals: Methylamine and Water Adsorption on PbS. *Phys. Rev. Lett.* **2010**, *104*, 116101.
(38) Deringer, V. L.; Dronskowski, R. Stabilities and reconstruction of clean PbS and PbSe surfaces: DFT results and the role of dispersion forces. *J. Phys. Chem. C* **2016**, *120*, 8813−8820.
(39) Yeon, D. H.; Lee, S. M.; Jo, Y. H.; Moon, J.; Cho, Y. S. Origin of the enhanced photovoltaic characteristics of PbS thin film solar cells processed at near room. *J. Mater. Chem. A* **2014**, *2*, 20112−20117.
(40) Monkhorst, H. J.; Pack, J. D. Special Points for Brillouin-Zone Integrations. *Phys. Rev. B* **1976**, *13*, 5188−5192.
(41) Bader, R. F. W. *Atoms in Molecules*; Oxford University Press: Oxford, 1990.
(42) Henkelman, G.; Arnaldsson, A.; Jónsson, H. A fast and robust algorithm for Bader decomposition of charge density. *Comput. Mater. Sci.* **2006**, *36*, 354−360.

https://dx.doi.org/10.1021/acs.langmuir.0c02425
Langmuir XXXX, XXX, XXX−XXX

(43) Tang, W.; Sanville, E.; Henkelman, G. A grid-based Bader analysis algorithm without lattice bias. *J. Phys.: Condens. Matter* **2009**, *21*, 084204.
(44) Rusu, P. C.; Brocks, G. Surface Dipoles and Work Functions of Alkylthiolates and Fluorinated Alkylthiolates on Au(111). *J. Phys. Chem. B* **2006**, *110*, 22628−22634.
(45) Crispin, X.; Geskin, V.; Crispin, A.; Cornil, J.; Lazzaroni, R.; Salaneck, W. R.; Brédas, J.-L. Characterization of the Interface Dipole at Organic/ Metal Interfaces. *J. Am.Chem. Soc.* **2002**, *124*, 8131−8141.
(46) Köhler, L.; Kresse, G. Density functional study of CO on Rh(111). *Phys. Rev. B* **2004**, *70*, 165405.

https://dx.doi.org/10.1021/acs.langmuir.0c02425
Langmuir XXXX, XXX, XXX−XXX